Journal of Sound and Vibration (2003) **259**(1), 63–80
doi:10.1006/jsvi.2002.5181, available online at http://www.idealibrary.com on IDEAL®

FREE VIBRATION OF ORTHOTROPIC SQUARE PLATES WITH A SQUARE HOLE

T. Sakiyama, M. Huang, H. Matsuda and C. Morita

Department of Structural Engineering, Nagasaki University, Bonkyo Machi 1-14*, Nagasaki* 852*, Japan. E-mail: sakiyama@st.nagasaki-u.ac.jp*

(*Received* 29 *August* 2001, *and in final form* 12 *February* 2002)

An approximate method is extended for analyzing the free vibration problem of orthotropic square plate with a square hole. In this paper, a square plate with a square hole is transformed into an equivalent square plate with non-uniform thickness by considering the hole as an extremely thin part of the equivalent plate. Therefore, the dynamic characteristics of a plate with a hole can be obtained by analyzing the equivalent plate. The Green function, which is the discrete solution for the deflection of the equivalent plate, is used to obtain the characteristic equation of the free vibration. The effects of the side to thickness ratio, hole side to plate side ratio and the variation of the thickness on the frequencies are considered. Some numerical analyses are carried out for the simply supported orthotropic square plate with a square hole. The efficiency and accuracy of the numerical solutions by the present method are investigated.

1. INTRODUCTION

Plates with holes are extensively used in aeronautical, mechanical and civil structures. Their dynamic characteristics have been studied for many years. Early studies were compiled by Leissa [1]. Paramasivam [2] extended a grid framework model to determine the effects of the holes on the fundamental frequencies. Numerical solutions were presented for isotropic square plates with square holes. Hegarty and Ariman [3] used a least-squares point-matching method to investigate the free vibration of the isotropic rectangular plates with a central circular hole. Clamped and simply supported plates were considered. The Rayleigh method was used to analyze the dynamic characteristics of plates with holes by Ali and Atwal [4]. Frequencies were shown for the isotropic simply supported square plates with square and rectangular holes. Aksu and Ali [5] proposed a finite difference formulation for the prediction of dynamic behaviour of isotropic rectangular plates with holes. Experimental and theoretical frequencies were given for the plates with single hole or double holes. Compared with the study of isotropic plates with holes, the analyses of orthotropic plates with holes are very limited. Reddy [6] studied the large-amplitude free vibration of layered composite plates with rectangular cutouts by finite element method. Frequencies corresponding to linear and non-linear situations were presented for thin and thick orthotropic and composite plates. Avalos *et al*. [7] obtained the frequency parameters for anisotropic rectangular plates with free-edge holes by using the Rayleigh–Ritz method. The effects of aspect ratio, hole side to plate side ratio and the position of the hole on the frequencies were investigated.

This paper extends the early work [8] to analyze the free vibration of orthotropic square plates with a hole. By considering the hole as an extremely thin part of a plate, the free

0022-460X/02/$35.00

vibration problem of a plate with a hole can be transformed into the free vibration problem of its equivalent square plates with non-uniform thickness. The Green function is used to obtain the characteristic equation of the free vibration. The effects of side to thickness ratio, hole side to plate side ratio and the variation of the thickness in one direction or two directions on the frequencies are presented. The lowest 10 frequency parameters and their mode shapes are given for simply supported orthotropic square plates with a square hole. By comparing the present results with those previously reported, the convergence and accuracy of the present method are investigated.

2. DISCRETE GREEN FUNCTION

An xyz co-ordinate system is used in the present study with its $x-y$ plane contained in the middle plane of an orthotropic square plate and the z-axis perpendicular to the middle plane of the plate. The thickness and the length of the orthotropic square plate are h and a respectively. The principal material axes of the plate in the direction of longitudinal, transverse and normal directions are designated as 1, 2 and 3. The differential equations of the plate with a concentrated load $\bar{P}$ at point (x_q, y_r) are as follows:

$$\frac{\partial Q_x}{\partial x}+\frac{\partial Q_y}{\partial y}=-\bar{P}\delta(x-x_q)\delta(y-y_r), \quad \frac{\partial M_x}{\partial x}+\frac{\partial M_{xy}}{\partial y}-Q_x=0,$$

$$\frac{\partial M_y}{\partial y}+\frac{\partial M_{xy}}{\partial x}-Q_y=0, \quad M_x=D_{11}\frac{\partial \theta_x}{\partial x}+D_{12}\frac{\partial \theta_y}{\partial y}+D_{16}\left(\frac{\partial \theta_x}{\partial y}+\frac{\partial \theta_y}{\partial x}\right),$$

$$M_y=D_{12}\frac{\partial \theta_x}{\partial x}+D_{22}\frac{\partial \theta_y}{\partial y}+D_{26}\left(\frac{\partial \theta_x}{\partial y}+\frac{\partial \theta_y}{\partial x}\right),$$

$$M_{xy}=D_{16}\frac{\partial \theta_x}{\partial x}+D_{26}\frac{\partial \theta_y}{\partial y}+D_{66}\left(\frac{\partial \theta_x}{\partial y}+\frac{\partial \theta_y}{\partial x}\right),$$

$$Q_y=kA_{44}\left(\frac{\partial w}{\partial y}+\theta_y\right)+kA_{45}\left(\frac{\partial w}{\partial x}+\theta_x\right),$$

$$Q_x=kA_{45}\left(\frac{\partial w}{\partial y}+\theta_y\right)+kA_{55}\left(\frac{\partial w}{\partial x}+\theta_x\right), \tag{1}$$

where Q_x and Q_y are the transverse shear forces, M_x and M_y are the bending moments, M_{xy} is the twisting moment, $k=5/6$ is the shear correction factor, $\delta(x-x_q)$ and $\delta(y-y_r)$ are Dirac's delta functions, A_{ij} is the extensional stiffness $(i,j=4,5)$ and D_{ij} is the bending stiffness $(i,j=1,2,6)$.

A_{ij}, D_{ij} can be obtained by the following expressions:

$$A_{ij}=\bar{Q}_{ij}h, \quad D_{ij}=\tfrac{1}{12}\bar{Q}_{ij}h^3,$$
$$\bar{Q}_{11}=Q_{11}, \quad \bar{Q}_{12}=Q_{12}, \quad \bar{Q}_{16}=0,$$
$$\bar{Q}_{22}=Q_{22}, \quad \bar{Q}_{26}=0, \quad \bar{Q}_{66}=Q_{66},$$
$$\bar{Q}_{44}=Q_{44}, \quad \bar{Q}_{45}=0, \quad \bar{Q}_{55}=Q_{55},$$
$$Q_{11}=\frac{E_1}{1-v_{12}v_{21}}, \quad Q_{22}=\frac{E_2}{1-v_{12}v_{21}}, \quad Q_{12}=\frac{v_{12}E_2}{1-v_{12}v_{21}},$$
$$Q_{44}=G_{23}, \quad Q_{55}=G_{31}, \quad Q_{66}=G_{12},$$

where E_1 is the axial modulus in the 1-direction, E_2 is the axial modulus in the 2-direction, v_{12} is the Poisson ratio associated with loading in the 1-direction and strain in the 2-direction, v_{21} is the Poisson ratio associated with loading in the 2-direction and strain in the 1-direction and G_{23}, G_{31} and G_{12} are the shear moduli in 2–3, 3–1 and 1–2 planes.

By using the non-dimensional expressions

$$[X_1, X_2] = \frac{a^2}{D_0(1 - v_{12}v_{21})}[Q_y, Q_x], \quad [X_3, X_4, X_5] = \frac{a}{D_0(1 - v_{12}v_{21})}[M_{xy}, M_y, M_x],$$
$$[X_6, X_7, X_8] = \left[\theta_y, \theta_x, \frac{w}{a}\right], \quad [\eta, \zeta, \xi] = \left[\frac{x}{a}, \frac{y}{a}, \frac{z}{h}\right],$$

the equation (1) can be rewritten as

$$\sum_{s=1}^{8}\left\{F_{1ts}\frac{\partial X_s}{\partial \zeta} + F_{2ts}\frac{\partial X_s}{\partial \eta} + F_{3ts}X_s\right\} + P\delta(\eta - \eta_q)\delta(\zeta - \xi_r)\delta_{1t} = 0, \tag{2}$$

where $t = 1{-}8$, $P = \bar{P}a/(D_0(1 - v_{12}v_{21}))$, $D_0 = Eh_0^3/12(1 - v_{12}v_{21})$ is the standard bending rigidity, h_0 is the standard thickness of the plate, δ_{ij} is Kronecker's delta, and F_{1ts}, F_{2ts} and F_{3ts} are given in Appendix A.

By dividing a rectangular plate vertically into m equal-length parts and horizontally into n equal-length parts as shown in Figure 1, the plate can be considered as a group of discrete points which are the intersections of the $(m + 1)$ vertical and $(n + 1)$ horizontal dividing lines. In this paper, the rectangular area, $0 \leqslant \eta \leqslant \eta_i$, $0 \leqslant \zeta \leqslant \zeta_j$, corresponding to the arbitrary intersection (i,j) as shown in Figure 1 is denoted as the area $[i,j]$, the intersection (i,j) denoted by $\bigcirc$ is called the main point of the area $[i,j]$, the intersections denoted by $\circ$ are called the inner dependent points of the area, and the intersections denoted by $\bullet$ are called the boundary dependent points of the area.

By integrating equation (2) over the area $[i,j]$, the following integral equation is obtained:

$$\sum_{s=1}^{8}\left\{F_{1ts}\int_0^{\eta_i}[X_s(\eta, \zeta_j) - X_s(\eta, 0)]\,\mathrm{d}\eta + F_{2ts}\int_0^{\zeta_j}[X_s(\eta_i, \zeta) = X_s(0, \zeta)]\,\mathrm{d}\zeta\right.$$
$$\left. + F_{3ts}\int_0^{\eta_i}\int_0^{\zeta_j} X_s(\eta, \zeta)\,\mathrm{d}\eta\,\mathrm{d}\zeta\right\} + Pu(\eta - \eta_q)u(\zeta - \zeta_r)\delta_{1t} = 0, \tag{3}$$

where $u(\eta - \eta_q)$ and $u(\zeta - \zeta_r)$ are the unit step functions.

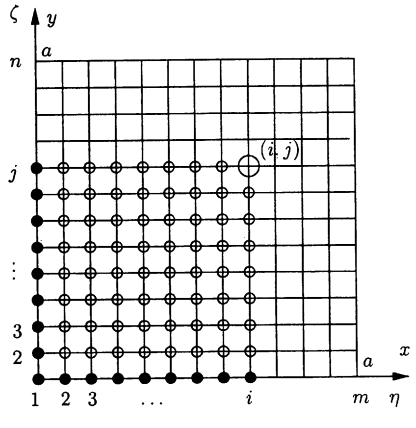

Figure 1. Discrete points on a rectangular plate.

Next, by applying the numerical integration method, the simultaneous equation for the unknown quantities $X_{sij} = X_s(\eta_i, \zeta_j)$ at the main point (i,j) of the area $[i,j]$ is obtained as follows:

$$\sum_{s=1}^{8}\left\{F_{1ts}\sum_{k=0}^{i}\beta_{ik}(X_{skj}-X_{sk0})+F_{2ts}\sum_{l=0}^{j}\beta_{jl}(X_{sil}-X_{s0l})+F_{3ts}\sum_{k=0}^{i}\sum_{l=0}^{j}\beta_{ik}\beta_{jl}X_{skl}\right\}+Pu_{iq}u_{jr}\delta_{1t}=0, \tag{4}$$

where $\beta_{ik}=\alpha_{ik}/m$, $\beta_{jl}=\alpha_{jl}/n$, $\alpha_{ik}=1-(\delta_{0k}+\delta_{ik})/2$, $\alpha_{jl}=1-(\delta_{0l}+\delta_{jl})/2$, $t=1-8$, $i=1-m$, $j=1-n$, $u_{iq}=u(\eta_i-\eta_q)$ and $u_{jr}(\zeta_j-\zeta_r)$.

The solution X_{pij} of the simultaneous equation (4) is obtained as follows:

$$X_{pij}=\sum_{t=1}^{8}\left\{\sum_{k=0}^{i}\beta_{ik}A_{pt}[X_{tk0}-X_{tkj}(1-\delta_{ik})]+\sum_{l-0}^{j}\beta_{jl}B_{pt}[X_{t0l}-X_{til}(1-\delta_{jl})]+\sum_{k=0}^{i}\sum_{l=0}^{j}\beta_{ik}\beta_{jl}C_{ptkl}X_{tkl}(1-\delta_{ik}\delta_{jl})\right\}-A_{pl}Pu_{iq}u_{jr}, \tag{5}$$

where $p=1-8$, A_{pt}, B_{pt} and C_{ptkl} are given in Appendix B.

In equation (5), the quantity X_{pij} at the main point (i,j) of the area $[i,j]$ is related to the quantities X_{tk0}, X_{t0l} at the boundary dependent points of the area and the quantities X_{tkj}, X_{til} and X_{tkl} at the inner dependent points of the area. With the spreading of the area $[i,j]$ according to the regular order as [1, 1], [1, 2],...,[1, n], [2, 1], [2, 2],...,[2 n],...,[m, 1], [m, 2],...,[m, n], a main point of the smaller area becomes one of the inner dependent points of the following larger areas. Whenever the quantity X_{pij} at the main point (i,j) is obtained by using equation (5) in the above-mentioned order, the quantities X_{tkj}, X_{til} and X_{tkl} at the inner dependent points of the following larger areas can be eliminated by substituting the obtained results into the corresponding terms on the right side of equation (5).

By repeating this process, the equation X_{pij} at the main point is only related to the quantities $X_{rk0}(r=1,3,4,6,7,8)$ and $X_{s0l}(s=2,3,5,6,7,8)$ which are six independent quantities at each boundary dependent point along the horizontal axis and the vertical axis in Figure 1 respectively. The result is

$$X_{pij}=\sum_{d=1}^{6}\left\{\sum_{f=0}^{i}a_{pijfd}X_{rf0}+\sum_{g=0}^{j}b_{pijgd}X_{s0g}\right\}+\bar{q}_{pij}P, \tag{6}$$

where a_{pijfd}, b_{pijgd} and $\bar{q}_{pij}$ are given in Appendix C.

Equation (6) gives the discrete solution of the fundamental differential equation (2) of the bending problem of a plate under a concentrated load, and the discrete Green function is chosen as $X_{8ij}/[\bar{P}a/D_0(1-\nu_{12}\nu_{21})]$.

3. INTEGRAL CONSTANT AND BOUNDARY CONDITION OF A RECTANGULAR PLATE

The integral constants X_{rfo} and X_{sog} involved in discrete solution (6) are all quantities at the discrete points along the edges $\zeta=0$ ($y=0$) and $\eta=0$ ($x=0$) of the rectangular plate. There are six integral constants at each discrete point. Half of them are self-evident according to the boundary conditions along the edges $\zeta=0$ and $\eta=0$ and half of them are needed to determine by the boundary conditions along the edges $\zeta=1$ and $\eta=1$.

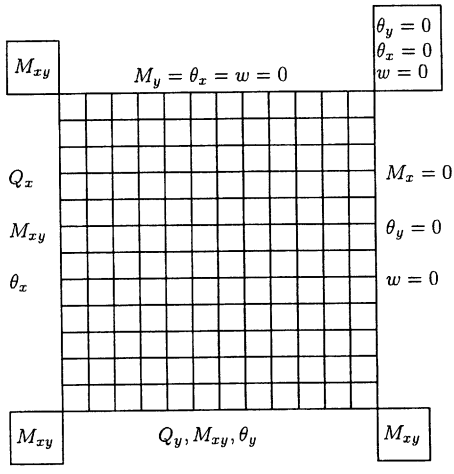

Figure 2. Simply supported plate.

The integral constants and the boundary conditions for a simply supported plate are shown in Figure 2, and those at the corners of the plate are shown in the boxes.

4. EQUIVALENT SQUARE PLATE OF A SQUARE PLATE WITH A HOLE

A square plate with a hole can be transformed into an equivalent square plate with non-uniform thickness (shown in Figure 3) by considering the hole as an extremely thin part of the plate theoretically. The thickness of the actual part of original square plate is expressed as h, and the thickness of the extremely thin part of the equivalent square plate is expressed as h_t. The thickness of the plate along the border line between the actual part and the extremely thin part is chosen as $(h + h_t)/2$. In this paper, numerical results are carried out for a simply supported square plate with a central square hole. The simply supported and free edges are denoted by the symbols S and F, respectively, and shown by solid line and dotted line.

5. CHARACTERISTIC EQUATION OF FREE VIBRATION OF SQUARE PLATE WITH NON-UNIFORM THICKNESS

By applying the Green function $w(x_0, y_0, x, y)/\bar{P}$ which is the displacement at a point (x_0, y_0) of a plate with a concentrated load $\bar{P}$ at the point (x, y), the displacement amplitude $\hat{w}(x_0, y_0)$ at a point (x_0, y_0) of the square plate during the free vibration is given as follows:

$$\hat{w}(x_0, y_0) = \int_0^a \int_0^a \rho h \omega^2 \hat{w}(x, y)[w(x_0, y_0, x, y)/\bar{P}]\, \mathrm{d}x\, \mathrm{d}y, \tag{7}$$

where ρ is the mass density of the plate material.

The following non-dimensional expressions are used:

$$\lambda^4 = \frac{\rho_0 h_0 \omega^2 a^4}{D_0(1 - v_{12}v_{21})}, \quad H(\eta, \zeta) = \frac{\rho(x, y)}{\rho_0}\frac{h(x, y)}{h_0}, \quad W(\eta, \zeta) = \frac{\hat{w}(x, y)}{a},$$

$$G(\eta_0, \zeta_0, \eta, \zeta) = \frac{w(x_0, y_0, x, y)}{a}\frac{D_0(1 - v_{12}v_{21})}{\bar{P}a},$$

where ρ_0 is the standard mass density.

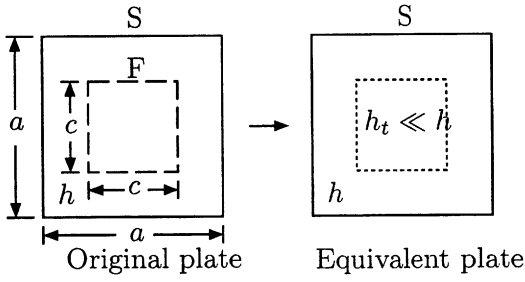

Figure 3. Square plate with a square hole and its equivalent square plate.

By using the numerical integration method, equation (7) is discretely expressed as

$$kW_{kl} = \sum_{i=0}^{m}\sum_{j=0}^{n} \beta_{mi}\beta_{nj}H_{ij}G_{klij}W_{ij}, \quad k = 1/(\mu\lambda^4). \tag{8}$$

From equation (8), homogeneous linear equations in $(m+1)\times(n+1)$ unknowns $W_{00}, W_{01}, \ldots, W_{0n}, W_{10}, W_{11}, \ldots, W_{1n}, \ldots, W_{m0}, W_{m1}, \ldots, W_{mn}$ are obtained as follows:

$$\sum_{i=0}^{m}\sum_{j=0}^{n}(\beta_{mi}\beta_{nj}H_{ij}G_{klij} - k\delta_{ik}\delta_{jl})W_{ij} = 0 \quad (k = 0, 1, \ldots, m,\ l = 0, 1, \ldots, n). \tag{9}$$

The characteristic equation of the free vibration of a square plate with variable thickness is obtained from equation (9) as follows:

$$\begin{vmatrix} \mathbf{K}_{00} & \mathbf{K}_{00} & \mathbf{K}_{00} & \ldots & \mathbf{K}_{0m} \\ \mathbf{K}_{10} & \mathbf{K}_{11} & \mathbf{K}_{12} & \ldots & \mathbf{K}_{1m} \\ \mathbf{K}_{20} & \mathbf{K}_{21} & \mathbf{K}_{22} & \ldots & \mathbf{K}_{2m} \\ \vdots & \vdots & \vdots & \ddots & \vdots \\ \mathbf{K}_{m0} & \mathbf{K}_{m1} & \mathbf{K}_{m2} & \ldots & \mathbf{K}_{mm} \end{vmatrix} = 0, \tag{10}$$

where

$$\mathbf{K}_{ij} = \beta_{mj}\begin{bmatrix} \beta_{n0}H_{j0}G_{i0j0} - k\delta_{ij} & \beta_{n1}H_{j1}G_{i0j1} & \ldots & \beta_{nn}H_{jn}G_{i0jn} \\ \beta_{n0}H_{j0}G_{i1j0} & \beta_{n1}H_{j1}G_{i1j1} - k\delta_{ij} & \ldots & \beta_{nn}H_{jn}G_{i1jn} \\ \beta_{n0}H_{j0}G_{i2j0} & \beta_{n1}H_{j1}G_{i2j1} & \ldots & \beta_{nn}H_{jn}G_{i2jn} \\ \vdots & \vdots & \vdots & \vdots \\ \beta_{n0}H_{j0}G_{inj0} & \beta_{n1}H_{j1}G_{inj1} & \ldots & \beta_{nn}H_{jn}G_{injn} - k\delta_{ij} \end{bmatrix}.$$

6. NUMERICAL RESULTS

6.1. CONVERGENCE OF THE SOLUTION

In order to examine the convergence, numerical calculation is carried out by varying the number of divisions m and n. The lowest 10 natural frequency parameters of an orthotropic square plate with a square hole are shown in Figure 4. The properties of the orthotropic material are given as $E_1/E_2 = 40$, $G_{12}/E_2 = 0{\cdot}5$, $G_{13} = G_{23} = G_{12}$, $\nu_{12} = 0{\cdot}25$. It can be noticed that convergent results of frequency parameter can be obtained by using Richardson's extrapolation formula for two cases of divisional numbers

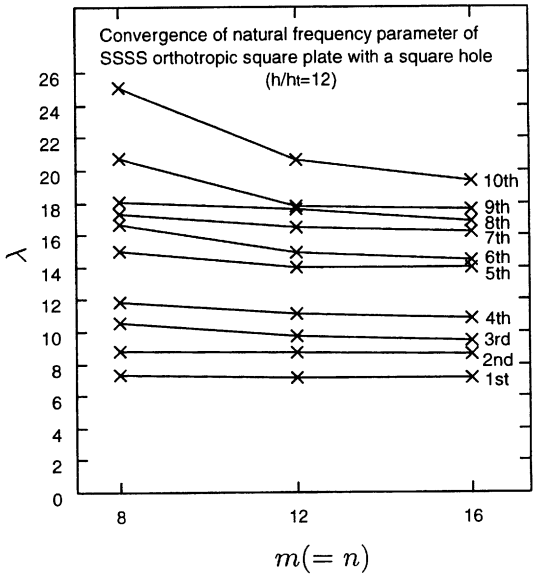

Figure 4. The natural frequency parameter λ versus the divisional number $m\,(=n)$ for the SSSS orthotropic square plate with a square hole and uniform thickness.

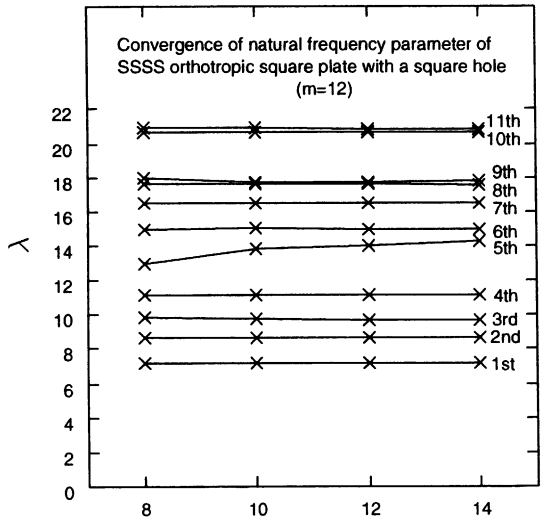

Figure 5. The natural frequency parameter λ versus the thickness ratio h/h_t for the SSSS orthotropic square plate with a square hole and uniform thickness.

$m\,(=n)$ of 12 and 16. Figure 5 is used to determine the suitable thickness ratio h/h_t of the original and extremely thin parts. It is sufficient to set the thickness ratio $h/h_t = 12$.

By the same method, the number of divisions $m\,(=n)$ and the thickness ratio h/h_t can be determined for the other plates. The convergent values of frequency parameter are obtained by using Richardson's extrapolation formula for two cases of divisional numbers $m\,(=n)$.

TABLE 1

Natural frequency parameter λ for SSSS isotropic square plate with a square hole and uniform thickness ($c/a = 0{\cdot}5$, $a/h = 100$, $h/h_t = 12$)

References	Mode sequence number									
	1st	2nd	3rd	4th	5th	6th	7th	8th	9th	10th
Present										
12×12	4·731	6·595	6·595	8·818	9·531	11·552	11·552	12·757	15·112	15·174
16×16	4·779	6·525	6·527	8·676	9·244	11·225	11·237	12·553	14·422	14·763
Ex.[†]	4·839	6·435	6·440	8·492	8·875	10·805	10·831	12·291	13·534	14·234
Reference [4]	4·936	6·502	6·502	8·525	8·813	—	—	—	—	—
Reference [6]	4·962	—	—	—	8·871	—	—	—	—	—

[†]The result obtained by Richardson's extrapolation formula.

6.2. ACCURACY OF THE SOLUTION

The frequencies of the free vibration of square plates with square holes are given to show the accuracy of the numerical solution obtained by the present method. The lowest 10 natural frequencies and mode shapes of these plates are presented for the cases of uniform thickness and variable thickness.

6.2.1. *Plate with uniform thickness*

Numerical values for the lowest 10 natural frequency parameter λ of the SSSS isotropic thin square plate with a square hole of side ratio $c/a = 0{\cdot}5$ and $\nu = 0{\cdot}3$ are given in Table 1 with the other values obtained by Ali and Atwal [4] and Reddy [6]. From Table 1, it can be seen that these values are in close agreement. The nodal patterns of the 10 modes of the plate are shown in Figure 6. Those of the fourth and fifth modes can also found in mode shapes of a plate without a hole [13, 14].

The effects of the hole size on the first five frequencies are shown in Figure 7 for the SSSS isotropic thin square plate. It might be noted that the variations of the fundamental and higher frequencies are different. As the ratio c/a increases, the fundamental frequency first decreases a little, then increases. For $c/a = 0{\cdot}5$, the fundamental frequency of the plate is higher than the corresponding frequency for the plate without a hole. But as the ratio c/a increases, the second, third and fourth frequencies first increase a little, then decreases. For $c/a = 0{\cdot}5$, these frequencies are lower than the corresponding frequencies for the plate without a hole. The fifth frequency monotonically decreases with the increase of c/a. To validate the accuracy of the present results, the finite element and the Rayleigh–Ritz results of Kaushal and Bhat [11] and the finite element results of Ali and Atwal [4] are also shown in Figure 7. These results agree closely for a small hole. As the hole size increases, the present results are in close agreement with the finite element results but quite lower than the Rayleigh–Ritz results for the higher frequencies.

Tables 2 and 3 present the numerical results for the lowest 10 natural frequency parameter λ of the SSSS orthotropic thin and moderately thick square plates with a square hole of side ratio $c/a = 0{\cdot}5$. By comparing the results with the results of Reddy [6], the accuracy of the present results is investigated. These tables show that the side to thickness ratio a/h affects the frequency considerably. The nodal patterns of the 10 modes of the plates are shown in Figures 8 and 9. It can be noted that when a/h changes form 100 to 10, the first, second, fourth and fifth mode shapes do not change. The third, eighth and tenth

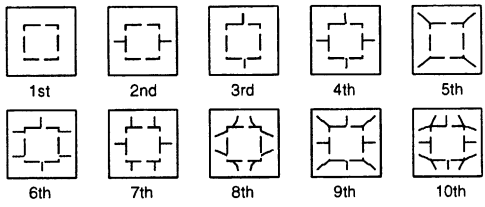

Figure 6. Nodal patterns for SSSS isotropic square plate with a square hole and uniform thickness ($c/a = 0{\cdot}5$, $a/h = 100$, $h/h_t = 12$).

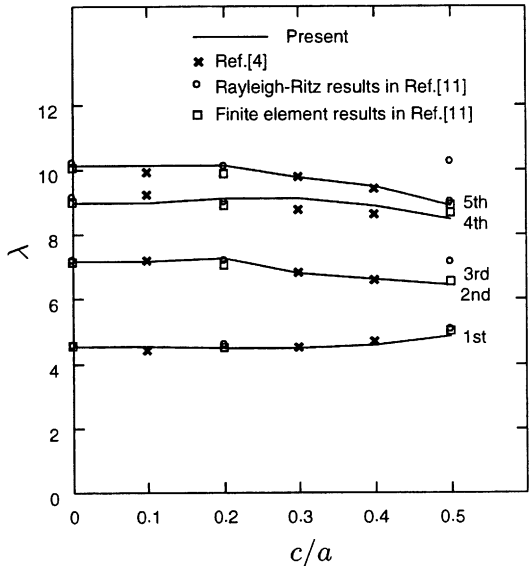

Figure 7. The first five frequencies versus the ratio c/a for SSSS isotropic square plate with a square hole and uniform thickness ($a/h = 100$).

TABLE 2

Natural frequency parameter λ for SSSS orthotropic square plate with a square hole and uniform thickness ($c/a = 0{\cdot}5$, $a/h = 100$, $h/h_t = 12$)

	Mode sequence number									
References	1st	2nd	3rd	4th	5th	6th	7th	8th	9th	10th
Present										
12×12	7·172	8·665	9·712	11·117	13·993	14·912	16·517	17·587	17·758	20·656
16×16	7·140	8·610	9·436	10·859	13·987	14·459	16·194	16·828	17·612	19·348
Ex.	7·098	8·539	9·070	10·528	13·979	13·877	15·778	15·853	17·425	17·666
Reference [6]	7·160	—	—	10·598	—	—	—	—	—	—

mode shapes change a lot. The sixth, seventh and ninth modes shapes in Figure 8 change into the seventh, sixth and eighth mode shapes in Figure 9 respectively. From Tables 1 and 2, it can be noted that the trend of the variation of the first frequency with the divisional number is different in Tables 1 and 2.

To better illustrate the effect of the hole size on the frequency of SSSS orthotropic thin and moderately thick plate, the variation of fundamental frequency with c/a is shown in

TABLE 3

Natural frequency parameter λ for SSSS orthotropic square plate with a square hole and uniform thickness ($c/a = 0{\cdot}5$, $a/h = 10$, $h/h_t = 12$)

References	Mode sequence number									
	1st	2nd	3rd	4th	5th	6th	7th	8th	9th	10th
Present										
12×12	6·494	7·726	8·196	9·763	10·664	12·293	13·079	14·275	14·778	14·851
16×16	6·485	7·685	8·041	9·534	10·721	12·115	12·641	13·781	14·534	14·627
Ex.	6·473	7·634	7·841	9·240	11·273	11·887	12·078	13·667	14·222	14·339
Reference [6]	6·537	—	—	9·139	—	—	—	—	—	—

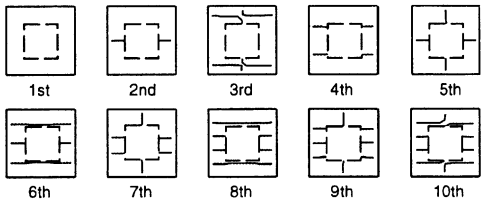

Figure 8. Nodal patterns for SSSS isotropic square plate with a square hole and uniform thickness ($c/a = 0{\cdot}5$, $a/h = 100$, $h/h_t = 12$).

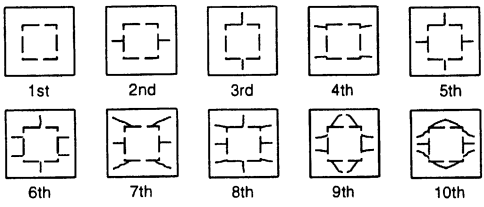

Figure 9. Nodal patterns for SSSS isotropic square plate with a square hole and uniform thickness ($c/a = 0{\cdot}5$, $a/h = 10$, $h/h_t = 12$).

Figure 10. It can be seen that the frequencies decrease with the increase of c/a for both thin and moderately thick plates. The effect of the transverse shear deformation on frequencies decrease with the increase of c/a. The present results agree closely with the results obtained by Lam *et al.* [12] and Reddy [6] shown in Figure 10. Comparing Figure 7 with Figure 10, it can be noted that the first natural frequency decreases a little first and then increases with c/a in Figure 7, while it decreases with c/a in Figure 10. To explain the phenomenon, two effects introduced by a hole are considered. The first one is a reduction in the strain energy of the plate which will decrease the frequency of the plate. The second one is a reduction in the mass which will increase the frequency. For the isotropic plate with a small hole, the first effect might be the dominant effect, and the frequency would decrease. But for a larger hole, the second effect might become the primary effect, and the frequency would begin to increase. Further explanation can be found in reference [4]. In this paper, no apparent decrease of the first frequency can be shown for isotropic plate. The first frequency decreases just a little first and then increases in Figure 7. For the orthotropic plate with a larger hole, the first effect might be still the dominant effect due to its high ratio of E_1/E_2, and the frequency would continue to decrease with $c/a \leqslant 0{\cdot}5$.

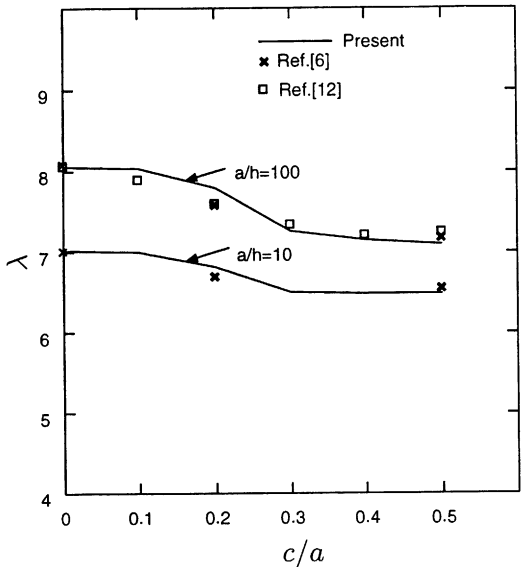

Figure 10. The fundamental frequencies versus the ratio c/a for SSSS orthotropic square plate with a square hole and uniform thickness.

Figure 11 shows the variation of the fundamental frequency parameter with the side to thickness ratio a/h for the plates with $c/a = 0$, 0·2 and 0·5. Isotropic and orthotropic cases are considered. The results of Reddy [6] are included in the figure.

It can be noticed that the effect of transverse shear deformation is much more pronounced in orthotropic plate than in isotropic plate. Also, the effect increases with the decrease of the ratio a/h. So as the ratio a/h increases, the fundamental frequencies show non-linear increase for values of a/h smaller than 30 but show linear increase for larger values of a/h and remain constant for large values of a/h. The fundamental frequency parameter for the plate with side ratio $c/a = 0{\cdot}2$ is lower than that of plate without a hole for both isotropic and orthotropic cases. Compared with the frequencies of the plates with $c/a = 0$ and 0·2, the frequency of the plate with $c/a = 0{\cdot}5$ is higher for the isotropic case but it is lower for the orthotropic case.

6.2.2. *Plate with variable thickness in one direction*

In order to investigate the accuracy of the present method for the plate with variable thickness, numerical values for the lowest 10 natural frequency parameter λ of the SSSS isotropic thin square plate with variable thickness in one direction are given in Table 4 with the results of Appl and Byers [10]. In this paper, variable thickness in one direction varies linearly along the y direction according to the equation $h(x, y) = h_0(1 + \alpha y/a)$. The cases of $\alpha = 0{\cdot}1$ and 0·8 are considered. The nodal patterns of the 10 modes of the plates are shown in Figure 12. With the increase of α, the horizontal nodal lines move down.

As application of the present method, the numerical results for the lowest 10 natural frequency parameter λ of the SSSS orthotropic thin and moderately thick square plates with a square hole of side ratio $c/a = 0{\cdot}5$ and variable thickness in one direction are presented in Tables 5 and 6. From these tables, it can be seen that the frequency parameters will increase with the increase of α. The nodal patterns of the 10 modes of the plates are shown in Figures 13 and 14. With the increase of α, the horizontal nodal lines move down in both figures. There is a change of mode order in the 10th mode in Figure 13.

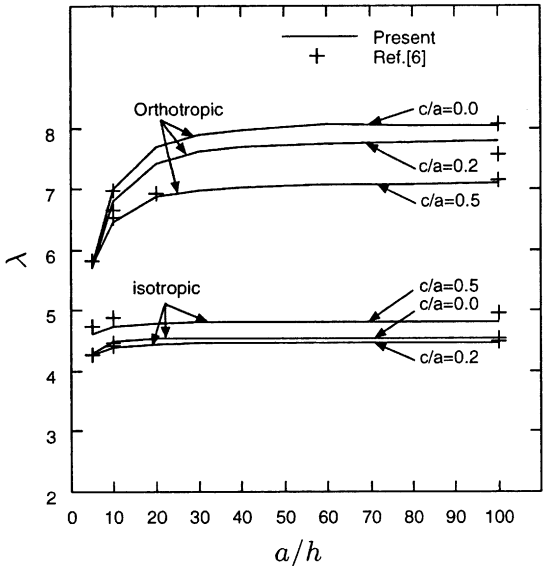

Figure 11. The fundamental frequency versus the thickness ratio a/h for SSSS square plate with a square hole and uniform thickness ($h/h_t = 12$).

TABLE 4

Natural frequency parameter λ for SSSS isotropic square plate with variable thickness in one direction ($a/h_0 = 100$, $h_0/h_t = 12$)

		Mode sequence number									
α	References	1st	2nd	3rd	4th	5th	6th	7th	8th	9th	10th
	Present										
0·1	12×12	4·687	7·512	7·513	9·540	10·928	10·932	12·406	12·407	14·871	14·725
	16×16	4·675	7·447	7·447	9·437	10·692	10·697	12·163	12·165	14·270	14·259
	Ex.	4·660	7·363	7·363	9·312	10·390	10·393	11·851	11·853	13·497	13·659
	Reference [10]	4·661	—	—	—	—	—	—	—	—	—
	Present										
0·8	12×12	5·387	8·578	8·614	10·949	12·347	12·520	14·222	14·277	16·591	16·910
	16×16	5·372	8·503	8·538	10·834	12·085	12·246	13·937	13·989	15·927	16·326
	Ex.	5·354	8·406	8·439	10·685	11·747	11·893	13·570	11·617	15·074	15·575
	Reference [10]	5·335	—	—	—	—	—	—	—	—	—

In Figure 14, other changes can be seen apparently in seventh, ninth and tenth mode shapes.

6.2.3. *Plate with variable thickness in two directions*

The numerical results for the lowest 10 natural frequency parameter λ of the SSSS orthotropic thin and moderately thick square with a square hole of side ratio $c/a = 0{\cdot}5$ and variable thickness in two directions are presented in Tables 7 and 8. The thickness of the plate varies in the x, y directions according to the sinusoidal function given by $h(x, y) = h_0(1 - \alpha \sin \pi x/a)(1 - \alpha \sin \pi y/a)$. Two cases of $\alpha = 0{\cdot}3$ and $0{\cdot}5$ are considered. It shows that the frequency parameters will decrease with the increase of α. The nodal

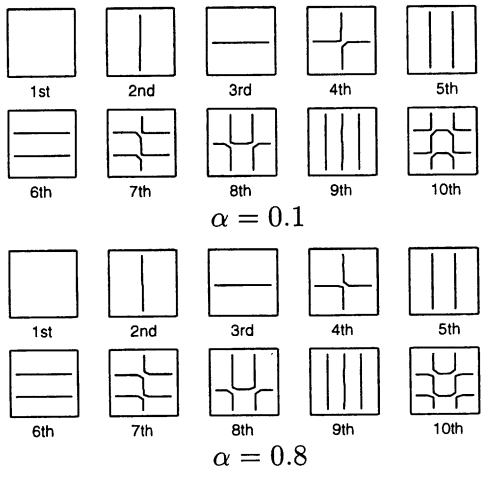

Figure 12. Nodal patterns for SSSS isotropic square plate with a variable thickness in one direction ($a/h = 100$, $h_0/h_t = 12$).

TABLE 5

Natural frequency parameter λ for SSSS orthotropic square plate with a square hole and variable thickness in one direction ($c/a = 0{\cdot}5$, $a/h_0 = 100$, $h_0/h_t = 12$)

		Mode sequence number									
α	References	1st	2nd	3rd	4th	5th	6th	7th	8th	9th	10th
	Present										
0·1	12 × 12	7·342	8·878	9·929	11·384	13·679	15·267	17·020	18·222	18·013	21·320
	16 × 16	7·309	8·821	9·654	11·121	13·839	14·802	16·583	17·275	17·235	19·808
	Ex.	7·267	8·749	9·299	10·782	14·045	14·204	16·020	16·056	16·234	17·865
	Present										
0·8	12 × 12	8·314	10·265	11·337	13·034	16·917	17·197	18·671	20·705	21·235	24·374
	16 × 16	8·272	10·197	11·002	12·752	16·389	16·627	18·127	19·718	20·791	22·808
	Ex.	8·217	10·110	10·571	12·388	15·710	15·894	17·427	18·448	20·221	20·794

TABLE 6

Natural frequency parameter λ for SSSS orthotropic square plate with a square hole and variable thickness in one direction ($c/a = 0{\cdot}5$, $a/h_0 = 10$, $h_0/h_t = 14$)

		Mode sequence number									
α	References	1st	2nd	3rd	4th	5th	6th	7th	8th	9th	10th
	Present										
0·1	12 × 12	6·604	7·848	8·268	9·898	11·569	12·367	13·221	14·295	14·823	14·996
	16 × 16	6·595	7·807	8·115	9·666	11·071	12·234	12·783	13·940	14·583	14·757
	Ex.	6·584	7·755	7·917	9·368	10·431	12·077	12·221	13·484	14·275	14·449
	Present										
0·8	12 × 12	7·214	8·547	8·880	10·700	11·574	13·069	13·902	17·337	15·070	15·700
	16 × 16	7·210	8·507	8·742	10·460	11·228	12·932	13·506	14·880	14·833	15·354
	Ex.	7·206	8·456	8·565	10·151	10·784	12·756	12·998	14·528	14·528	14·947

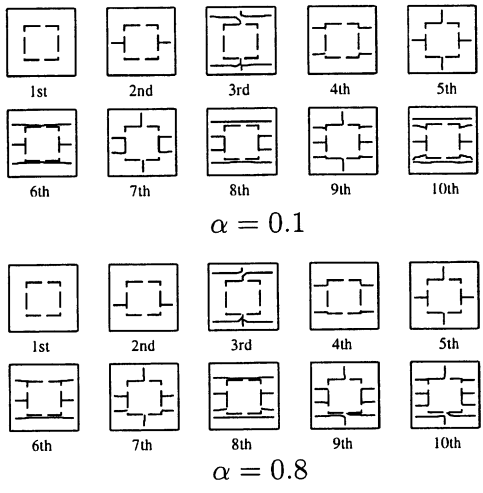

Figure 13. Nodal patterns for SSSS orthotropic square plate with a square hole and variable thickness in one direction ($c/a = 0{\cdot}5$, $a/h = 100$, $h_0/h_t = 12$).

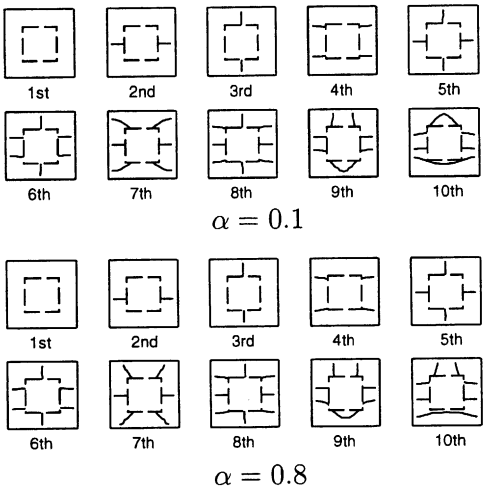

Figure 14. Nodal patterns for SSSS orthotropic square plate with a square hole and variable thickness in one direction ($c/a = 0{\cdot}5$, $a/h = 10$, $h_0/h_t = 14$).

patterns of the 10 modes of the plates are shown in Figures 15 and 16. From Figures 8, 13 and 15, it can be found that the first nine mode shapes are similar. The 10th mode shape in Figure 8 is similar to that for $\alpha = 0{\cdot}8$ in Figure 13. The 10th mode shape for $\alpha = 0{\cdot}1$ in Figure 13 is similar to those of $\alpha = 0{\cdot}3$ and $0{\cdot}5$ in Figure 15. With the increase of α, only the nodal lines of mode shape in Figure 13 move down, but those in Figure 15 do not. This is because the thickness at two symmetric points with regard to horizontal axis is different in Figure 13 but the same in Figure 15. From Figures 9, 14 and 16, it can be noticed that the first eight mode shapes are similar. The ninth and tenth mode shapes in Figure 9 are similar to those in Figure 14 but different from those in Figure 15.

TABLE 7

Natural frequency parameter λ for SSSS orthotropic square plate with a square hole and variable thickness in two directions ($c/a = 0{\cdot}3$, $a/h_0 = 100$, $h_0/h_t = 14$)

		Mode sequence number									
α	References	1st	2nd	3rd	4th	5th	6th	7th	8th	9th	10th
	Present										
0·3	12×12	6·315	7·727	8·813	10·027	12·848	13·305	15·682	14·773	16·050	18·619
	16×16	6·304	7·686	8·582	9·831	12·704	12·935	15·001	14·494	15·594	17·341
	Ex.	6·289	7·634	8·286	9·578	12·520	12·461	14·125	14·135	15·007	15·698
	Present										
0·5	12×12	5·680	7·059	8·177	9·277	11·786	12·184	13·365	14·337	14·746	17·026
	16×16	5·685	7·031	7·994	9·124	11·641	11·869	13·126	13·715	14·174	15·892
	Ex.	5·691	6·994	7·759	8·927	11·454	11·463	12·819	12·915	13·439	14·433

TABLE 8

Natural frequency parameter λ for SSSS orthotropic square plate with a square hole and variable thickness in two directions ($c/a = 0{\cdot}3$, $a/h_0 = 10$, $h_0/h_t = 16$)

		Mode sequence number									
α	References	1st	2nd	3rd	4th	5th	6th	7th	8th	9th	10th
	Present										
0·3	12×12	6·000	7·223	7·824	9·223	10·321	11·796	12·203	13·560	13·942	14·154
	16×16	5·996	7·190	7·684	9·033	10·189	11·630	11·937	13·117	13·588	13·833
	Ex.	5·995	7·147	7·504	8·788	10·021	11·416	11·467	12·548	13·133	13·420
	Present										
0·5	12×12	5·519	6·762	7·398	8·749	9·317	11·284	11·509	13·486	12·852	13·542
	16×16	5·530	6·737	7·278	8·594	9·509	11·127	11·220	12·566	12·490	13·061
	Ex.	5·543	6·705	7·124	8·395	9·755	10·925	10·849	11·381	12·024	12·442

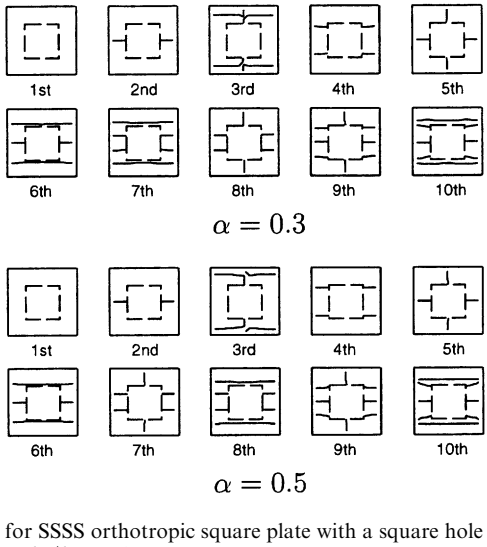

Figure 15. Nodal patterns for SSSS orthotropic square plate with a square hole and variable thickness in two direction ($c/a = 0{\cdot}5$, $a/h = 100$, $h_0/h_t = 14$).

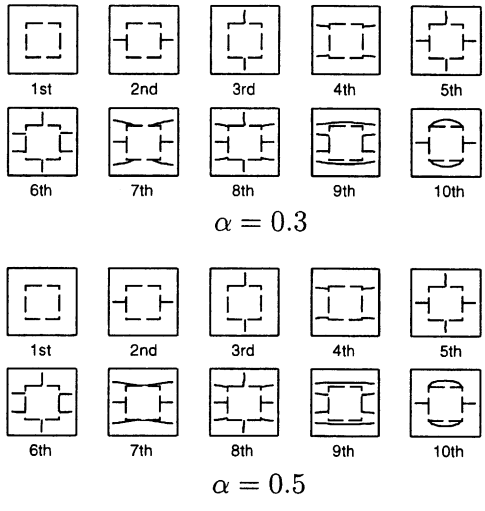

Figure 16. Nodal patterns for SSSS orthotropic square plate with a square hole and variable thickness in two direction ($c/a = 0{\cdot}5$, $a/h = 10$, $h_0/h_t = 16$).

7. CONCLUSIONS

An approximate method is extended for analyzing the free vibration problem of orthotropic square plate with a square hole. An equivalent square plate is used to obtain the dynamic characteristics of a plate with a hole. The characteristic equation of the free vibration is got by using the Green function. The frequency parameters and their mode shapes are shown for simply supported thin and moderately thick plates with a hole for isotropic and orthotropic cases. It can be known that the transverse shear deformation effect is much more pronounced in orthotropic plate than in isotropic plate. The effects of the variation of the thickness in one and two direction on the frequencies are considered. The results by the present method have been compared with those previously reported. It shows that the present results have a good convergence and satisfactory accuracy. Although numerical results are given for only simply supported plates, the present method is a general method and can be used to solve the vibration problem of plates with different boundary conditions.

ACKNOWLEDGMENTS

The present study was sponsored by the Japan Society for the Promotion of Science (JSPS).

REFERENCES

1. A. W. Leissa 1969 *Vibration of Plates* (NASA SP-160), Washington, DC: Office of Technology Utilization, NASA
2. P. Paramasivam 1973 *Journal of Sound and Vibration* **30**, 173–178. Free vibration of square plates with square openings.
3. R. F. Hegarty and T. Ariman 1975 *International Journal of Solids Structures* **11**, 895–906. Elasto-dynamic analysis of rectangular plates with circular holes.

4. R. Ali and S. J. Atwal 1980 *Computers and Structures* **12**, 819–823. Prediction of natural frequencies of vibration of rectangular plates with rectangular cutouts.
5. G. Aksu and R. Ali 1976 *Journal of Sound and Vibration* **44**, 147–158. Determination of dynamic characteristics of rectangular plates with cutouts using a finite difference formulation.
6. J. N. Reddy 1982 *Journal of Sound and Vibration* **83**, 1–10. Large amplitude flexural vibration of layered composite plates with cutouts.
7. D. R. Avalos, H. A. Larrondo and P. A. A. Laura 1999 *Journal of Sound and Vibration* **222**, 691–695. Analysis of vibrating rectangular anisotropic plate with free-edge holes.
8. M. Huang and T. Sakiyama 1999 *Journal of Sound and Vibration* **226**, 769–789. Free vibration analysis of rectangular plates with variously shaped holes.
9. G. Mundkur, R. B. Bhat and S. Neriya 1994 *Journal of Sound and Vibration* **176**, 136–144. Vibration of plates with cut-outs using boundary characteristic orthogonal polynomial functions in the Rayleigh–Ritz method.
10. F. C. Appl and N. R. Byers 1965 *Journal of Applied Mechanics* **32**, 163–167. Fundamental frequency of simply supported rectangular plates with linearly varying thickness.
11. A. Kaushal and R. B. Bhat 14*th Canadian Congress of Applied Mechanics CANCAM*'98. A comparative study of vibration of plates with cutouts using the finite element and the Rayleigh Ritz methods.
12. K. Y. Lam, K. C. Hung and S. T. Chow 1989 *Applied Acoustics* **28**, 49–60. Vibration analysis of plates with cutouts by the modified Rayleigh Ritz method.
13. G. N. Geannakakes 1995 *Journal of Sound and Vibration* **183**, 441–478. Natural frequencies of arbitrarily shaped plates using the Rayleigh–Ritz method together with natural co-ordinate regions and normalized characteristic orthogonal polynomials.
14. K. M. Liew, K. C. Hung and M. K. Clim 1995 *Journal of Sound and Vibration* **182**, 77–90. Vibration of mindlin plates using boundary characteristic orthogonal polynomials.
15. I. M. Daniel and O. Ishai 1994 *Engineering Mechanics of Composite Materials*. Oxford: Oxford University Press.

APPENDIX A

$$F_{111} = F_{123} = F_{134} = 1, \quad F_{146} = \bar{D}_{12}, \quad F_{147} = \bar{D}_{16}, \quad F_{156} = \bar{D}_{22},$$
$$F_{157} = F_{166} = \bar{D}_{26}, \quad F_{167} = \bar{D}_{66}, \quad F_{178} = k\bar{A}_{44}, \quad F_{188} = k\bar{A}_{45},$$
$$F_{212} = F_{225} = F_{233} = \mu, \quad F_{246} = F_{267} = \mu\bar{D}_{16}, \quad F_{247} = \mu\bar{D}_{11},$$
$$F_{256} = \mu\bar{D}_{26}, \quad F_{257} = \mu\bar{D}_{12}, \quad F_{266} = \mu\bar{D}_{66}, \quad F_{278} = F_{379} = F_{386} = \mu k\bar{A}_{45},$$
$$F_{288} = F_{387} = \mu k\bar{A}_{55}, \quad F_{322} = F_{331} = -\mu, \quad F_{345} = F_{354} = F_{363} = -\mu\bar{D},$$
$$F_{371} = F_{382} = -\mu\overline{DT}, \quad \text{other } F_{kts} = 0.$$

APPENDIX B

$$A_{p1} = \gamma_{p1}, \quad A_{p2} = 0, \quad A_{p3} = \gamma_{p2}, \quad A_{p4} = \gamma_{p3},$$
$$A_{p5} = 0, \quad A_{p6} = \bar{D}_{12}\gamma_{p4} + \bar{D}_{22}\gamma_{p5} + \bar{D}_{26}\gamma_{p6},$$
$$A_{p7} = \bar{D}_{16}\gamma_{p4} + \bar{D}_{26}\gamma_{p5} + \bar{D}_{66}\gamma_{p6}, \quad A_{p8} = k(\bar{A}_{44}\gamma_{p7} + \bar{A}_{45}\gamma_{p8}),$$
$$B_{p1} = 0, \quad B_{p2} = \mu\gamma_{p1}, \quad \beta_{p3} = \mu\gamma_{p3}, \quad B_{p4} = 0,$$
$$B_{p5} = \mu\gamma_{p2}, \quad B_{p6} = \mu(\bar{D}_{16}\gamma_{p4} + \bar{D}_{26}\gamma_{p5} + \bar{D}_{66}\gamma_{p6}),$$
$$B_{p7} = \mu(\bar{D}_{11}\gamma_{p4} + \bar{D}_{12}\gamma_{p5} + \bar{D}_{16}\gamma_{p6}), \quad B_{p8} = \mu k(\bar{A}_{45}\gamma_{p7} + \bar{A}_{55}\gamma_{p8}),$$
$$C_{p1kl} = \mu\gamma_{p3} + \mu\overline{DT}_{kl}\gamma_{p7}, \quad C_{p2kl} = \mu\gamma_{p2} + \mu\overline{DT}_{kl}\gamma_{p8},$$
$$C_{p3kl} = \mu\bar{D}_{kl}\gamma_{p6}, \quad C_{p4kl} = \mu\bar{D}_{kl}\gamma_{p7}, \quad C_{p5kl} = \mu\bar{D}_{kl}\gamma_{p4},$$

$$C_{p6kl} = -\mu k(\bar{A}_{44}\gamma_{p7} + \bar{A}_{45}\gamma_{p8}), \quad C_{p7kl} = -\mu k(\bar{A}_{45}\gamma_{p7} + \bar{A}_{55}\gamma_{p8}),$$
$$C_{p8kl} = 0, \quad [\gamma_{pt}] = [\rho_{tp}]^{-1}, \quad \rho_{11} = \beta_{ii}, \quad \rho_{12} = \mu\beta_{jj}, \quad \rho_{22} = -\mu\beta_{ij},$$
$$\rho_{23} = \beta_{ii}, \quad \rho_{25} = \mu\beta_{jj}, \quad \rho_{31} = -\mu\beta_{ij}, \quad \rho_{33} = \mu\beta_{jj}, \quad \rho_{34} = \beta_{ii},$$
$$\rho_{45} = -\mu\beta_{ij}\bar{D}_{ij}, \quad \rho_{46} = \bar{D}_{12}\beta_{ii} + \mu\bar{D}_{16}\beta_{jj}, \quad \rho_{47} = \bar{D}_{16}\beta_{ii} + \mu\bar{D}_{11}\beta_{jj},$$
$$\rho_{54} = -\mu\beta_{ij}\bar{D}_{ij}, \quad \rho_{56} = \bar{D}_{22}\beta_{ii} + \mu\bar{D}_{26}\beta_{jj}, \quad \rho_{57} = \bar{D}_{26}\beta_{ii} + \mu\bar{D}_{12}\beta_{jj},$$
$$\rho_{63} = -\mu\beta_{ij}\bar{D}_{ij}, \quad \rho_{66} = \bar{D}_{26}\beta_{ii} + \mu\bar{D}_{66}\beta_{jj}, \quad \rho_{67} = \bar{D}_{66}\beta_{ii} + \mu\bar{D}_{16}\beta_{jj},$$
$$\rho_{71} = -\mu\beta_{ij}\bar{D}_{ij}, \quad \rho_{76} = \mu k\bar{A}_{44}\beta_{ij}, \quad \rho_{77} = \mu k\bar{A}_{45}\beta_{ij}, \quad \rho_{78} = k(\bar{A}_{44}\beta_{ii} + \mu\bar{A}_{45}\beta_{jj}),$$
$$\rho_{82} = -\mu\beta_{ij}\bar{D}_{ij}, \quad \rho_{86} = \mu k\bar{A}_{45}\beta_{ij}, \quad \rho_{87} = \mu k\bar{A}_{55}\beta_{ij}, \quad \rho_{88} = k(\bar{A}_{45}\beta_{ii} + \mu\bar{A}_{55}\beta_{jj}),$$
$$\text{other} \quad \rho_{tp} = 0.$$

APPENDIX C

$$a_{1i0i1} = a_{3i0i2} = a_{4i0i3} = 1, \quad a_{6i0i4} = a_{7i0i5} = a_{8i0i6} = 1,$$

$$b_{20jj1} = b_{30jj2} = b_{50jj3} = 1, \quad b_{60jj4} = b_{70jj5} = b_{80jj6} = 1, \quad b_{30002} = 0,$$

$$a_{pijfd} = \sum_{t=1}^{13}\left\{\sum_{k=0}^{i}\beta_{ik}A_{pt}[a_{tk0fd} - a_{tkjfd}(1-\delta_{ki})] + \sum_{l=0}^{j}\beta_{jl}B_{pt}[a_{t0lfd} - a_{tilfd}(1-\delta_{lj})] + \sum_{k=0}^{i}\sum_{l=0}^{j}\beta_{ik}\beta_{jl}C_{ptkl}a_{tklfd}(1-\delta_{ki}\delta_{lj})\right\},$$

$$b_{pijfd} = \sum_{t=1}^{13}\left\{\sum_{k=0}^{i}\beta_{ik}A_{pt}[b_{tk0gd} - b_{tkjgd}(1-\delta_{ki})] + \sum_{l=0}^{j}\beta_{jl}B_{pt}[b_{t0lgd} - b_{tilgd}(1-\delta_{lj})] + \sum_{k=0}^{i}\sum_{l=0}^{j}\beta_{ik}\beta_{jl}C_{ptkl}b_{tklgd}(1-\delta_{ki}\delta_{lj})\right\},$$

$$\bar{q}_{pij} = \sum_{t=1}^{13}\left\{\sum_{k=0}^{i}\beta_{ik}A_{pt}[\bar{q}_{tk0} - \bar{q}_{tkj}(1-\delta_{ki})] + \sum_{l=0}^{j}\beta_{jl}B_{pt}[\bar{q}_{t0l} - \bar{q}_{til}(1-\delta_{lj})] + \sum_{k=0}^{i}\sum_{l=0}^{j}\beta_{ik}\beta_{jl}C_{ptkl} - A_{p1}u_{iq}u_{jr}\right\}.$$